nanomaterials

MDPI

Article

Structural, Electrical, and Optical Properties of SWCNTs Synthesized through Floating Catalyst Chemical Vapor Deposition

Melorina Dolafi Rezaee [a], Biplav Dahal [a], John Watt [b], Mahir Abrar [c], Deidra R. Hodges [c] and Wenzhi Li [a,*]

[a] Department of Physics, Florida International University, Miami, FL 33199
[b] Center for Integrated Nanotechnologies, Los Alamos National Laboratory, Los Alamos, NM, 87545
[c] Department of Electrical & Computer Engineering, Florida International University, Miami, FL 33174
* Correspondence: Wenzhi.Li@fiu.edu (W. Li)

Abstract: Single-walled carbon nanotube (SWCNT) thin films were synthesized by using a floating catalyst chemical vapor deposition (FCCVD) method with a low flow rate (200 sccm) of mixed gases (Ar and H_2). SWCNT thin films with different thicknesses can be prepared by controlling the collection time of the SWCNTs on membrane filters. Transmission electron microscopy (TEM) shows that the SWCNTs form bundles and SWCNTs have an average diameter of 1.46 nm. Raman spectra of the SWCNT films did not show the D-band indicating that the synthesized SWCNTs are very well-crystallized. Although the electrical properties of SWCNTs have been widely studied so far, the Hall effect of SWCNTs has not been fully studied to explore the electrical characteristics of SWCNT thin films. In this research, Hall effect measurements have been explored to investigate the important electrical characteristics of SWCNTs such as carrier mobility, carrier density, Hall coefficient, conductivity, and sheet resistance. The samples with transmittance between 95-43% showed a high carrier density of 10^{21}-10^{23} cm^{-3}. SWCNTs were also treated using Brønsted acids (HCl, HNO_3, H_2SO_4) to enhance their electrical properties. After the acid treatments, the samples maintain their p-type nature. The carrier mobility and conductivity increased and the sheet resistance decreased for all treated samples. The highest mobility of 1.5 cm^2/Vs was obtained through sulfuric acid treatment at 80 ^oC while the highest conductivity (30720 S/m) and lowest sheet resistance (43 ohm/square) were achieved through the nitric acid treatment at room temperature. Different functional groups were identified in our synthesized SWCNTs before and after the acid treatments using Fourier Transform Infrared Spectroscopy (FTIR).

Keywords: SWCNTs; FCCVD method; Raman spectroscopy; Hall effect measurements; Acid treatments; FTIR

1. Introduction

Carbon nanotubes (CNTs) are cylindrical molecules made of rolled-up sheets of single-layer carbon atoms (graphene) [1]. SWCNTs have diameters in the range of 1-2 nanometers (nm), double-walled carbon nanotubes (DWCNTs) have diameters in the range of 2-4 nm, and multi-walled carbon nanotubes (MWCNTs) have diameters in the range of few nanometers to hundred nanometers. MWCNTs consist of many concentrically stacked nanotubes with lengths of several micrometers or millimeters [2]. The credit for discovering MWCNTs and SWCNTs is given to Ijima [3,4] in 1991 and 1993, respectively.

Due to their lightweight and one-dimensional structure, SWCNTs show unique mechanical, electrical, optical, and thermal properties [5,6,7]. For example, their electrical conductivity is estimated theoretically as 10^8 S/m and they exhibit a high thermal conductivity of 3500 W/k.m. The theoretical tensile strength of the individual SWCNTs is around 100 GPa with Young's modulus of 1 TPa [8,9]. Because of these distinctive properties,

SWCNTs can be utilized in a wide range of applications, such as flexible and transparent microelectronics, energy storage and conversion devices, multifunctional composites, aerospace devices, electric conductors, etc. [10,11].

Compared to other methods like arc discharge or laser ablation, chemical vapor deposition (CVD) is one of the most favored techniques to synthesize SWCNTs due to its high yield, low impurity, and gentle synthesis conditions [12]. So far, different CVD processes have been introduced to fabricate SWCNTs, such as aerosol-assisted CVD [13], microwave plasma-enhanced CVD [14], hot-filament CVD [15], oxygen-assisted CVD [16], FCCVD, etc. Compared to the other CVD techniques, FCCVD is more appropriate for the mass production of SWCNTs because of its low cost, good flexibility, scalability, and controllability [17,18]. The properties of the SWCNT films strongly depend on the morphology of the SWCNTs' bundles, like their length, diameter, density, etc. [19], which can be efficiently controlled in the FCCVD technique.

In the FCCVD method, the appropriate choice of growth parameters plays an important role in controlling the growth of SWCNTs. Thiophene is commonly used to deliver sulfur components to the SWCNTs synthesis [20]. Sulfur plays a vital role in nucleation, renucleation, surface chemistry, and the aerogel formation of the catalyst nanoparticles. On the other hand, the catalyst affects the SWCNTs' morphology and helps the growth of the SWCNTs by reducing the synthesis energy [21]. Because of the low bonding energy between the sulfur and carbon atoms, thiophene decomposes earlier than ferrocene in the initial phase of the FCCVD reaction. The results of this process are hydrocarbon species and liberated sulfur atoms. A thin layer of coating is formed on the surface of the metallic catalyst by these liberated sulfur atoms. This is advantageous to the growth of SWCNTs because the sulfur surfactant can prevent the encapsulation of carbon particles. Moreover, it can stop the agglomeration between the sulfur-coated catalyst particles [22].

The type, morphology, and crystallinity of the synthesized SWCNTs can be determined by the carbon precursors such as ethanol. The carbon precursor is dissociated after being absorbed on the surface of the catalyst. A SWCNT cap is formed by the transformation of a closed carbon network. The SWCNT growth continues by generating carbon precipitation from the catalyst below the SWCNT cap. The growth stops after the termination of the catalysts [23] by the complete sulfur coverage on the surface of the catalyst particle [22,24]. SWCNT's diameter distribution is known to be affected by the composition of carrier gases. As an example, it was observed that increasing Ar as a carrier gas leads to a decrease in the SWCNTs diameter distributions [25]. A small diameter distribution is favorable for the reproductivity and consistency of SWCNT products.

Hydrogen is commonly used as a carrier gas in the FCCVD system. This gas is found to be very beneficial to the synthesis of SWCNTs. It can help the breakdown of the hydrocarbon precursors [26] and preserve the catalyst's lifetime [27]. SWCNTs can show either semiconducting or metallic behaviors depending on their chiral vector. The electronic properties of SWCNTs can be improved by doping using acid treatments. Brønsted acids (HCL, HNO_3, H_2SO_4, …) have been known to have electrochemical effects on graphite leading to acceptor doping [28,29].

In this work, we report the mass production of clean SWCNT films using the FCCVD method. We followed a process similar to Zhang et al.' [30] to synthesize SWCNTs with some changes in the type of carrier gases, their total flow rate, and the synthesis procedure. Our synthesis process with a total flow rate of the carrier gases at 200 sccm can be considered a low-cost procedure leading to the mass production of CNTs. In this research, thiophene (C_4H_4S) was used as a growth promoter, ferrocene as the catalyst, ethanol as the carbon precursor, and argon and hydrogen as the carrier gases. The morphology and characteristics of the thin films were examined through scanning electron microscopy (SEM) and transmission electron microscopy (TEM). Raman spectroscopy was used to show the quality and crystallinity of the SWCNT films. The transmittance of the synthesized SWCNT films was obtained for the thin film samples with collection times of 5, 10, 15, 20, and 25 minutes and the electronic properties of the synthesized SWCNTs were

investigated using the Hall effect measurements. The SWCNT films showed a high carrier concentration of 10^{21}-10^{23} cm^{-3} which is in good agreement with the theoretical prediction [31,32]. H_2SO_4, HCL, and HNO_3 were used for the treatment of the thin films, and the effect of different acid treatments on the mobility, conductivity, and sheet resistance of samples was studied. Fourier Transform Infrared Spectroscopy (FTIR) was employed to determine the functional groups in SWCNT films before and after the acid treatment.

2. Experimental

2.1. Materials

Ferrocene (98%, Aldrich) was used as a catalyst precursor. Thiophene (99+%, Acros Organics) and ethanol (89-91%, Fisher Chemical) were used as the growth promoter and the carbon source, respectively. Argon (AR UHP300, Airgas) and hydrogen (HY UHP300, Airgas) were employed as carrier gases. Millipore Express membrane filters (0.45 μm PES Membrane) were used to collect the SWCNTs. SWCNT thin films were doped using sulfuric acid (H_2SO_4, 96.1 w/w %, Fisher Scientific), nitric acid (HNO_3, 69.4 w/w %, Fisher Scientific), and hydrochloric acid (HCL, 37.2 w/w %, Fisher Scientific).

2.2. SWCNTs Synthesis

The precursor solution was prepared by dissolving ferrocene (0.4 wt %) and thiophene (molar ratio of S/Fe=0.3) in 10 milliliters of ethanol. A syringe pump was used to inject the precursor solution into a heating line kept at 140 °C. The feeding rate of the syringe pump was adjusted at 6 μl/min. The precursor solution was evaporated in the heating line and carried into a vertical furnace by argon and hydrogen gases, each with a flow rate of 100 standard cubic centimeters (sccm). The temperature of the furnace was kept at 1000 °C during the experiment. During the growth time (30 minutes) valve1 is kept open while valve2 and 3 are closed, so residual air in the reaction chamber and any initially produced materials during this time are exhausted through the oil trap (Fig.1). After that, valve 2 is opened and valve 1 is simultaneously closed to collect the pure and clean SWCNTs on a membrane filter, which is kept in a collection tube at room temperature. To increase the mass production of the CNTs, we added an extra valve (valve 3) (Fig.1). The SWCNT films can be removed from the collection tube after being purged with argon at 100 sccm, and a new membrane filter would be installed and purged with argon to get rid of the air inside the collection tube. Then, valve 2 would be opened and valves 1 and 3 closed to collect the SWCNTs again. This procedure can be repeated several times without stopping the experiment to produce several CNT thin films in one experiment.

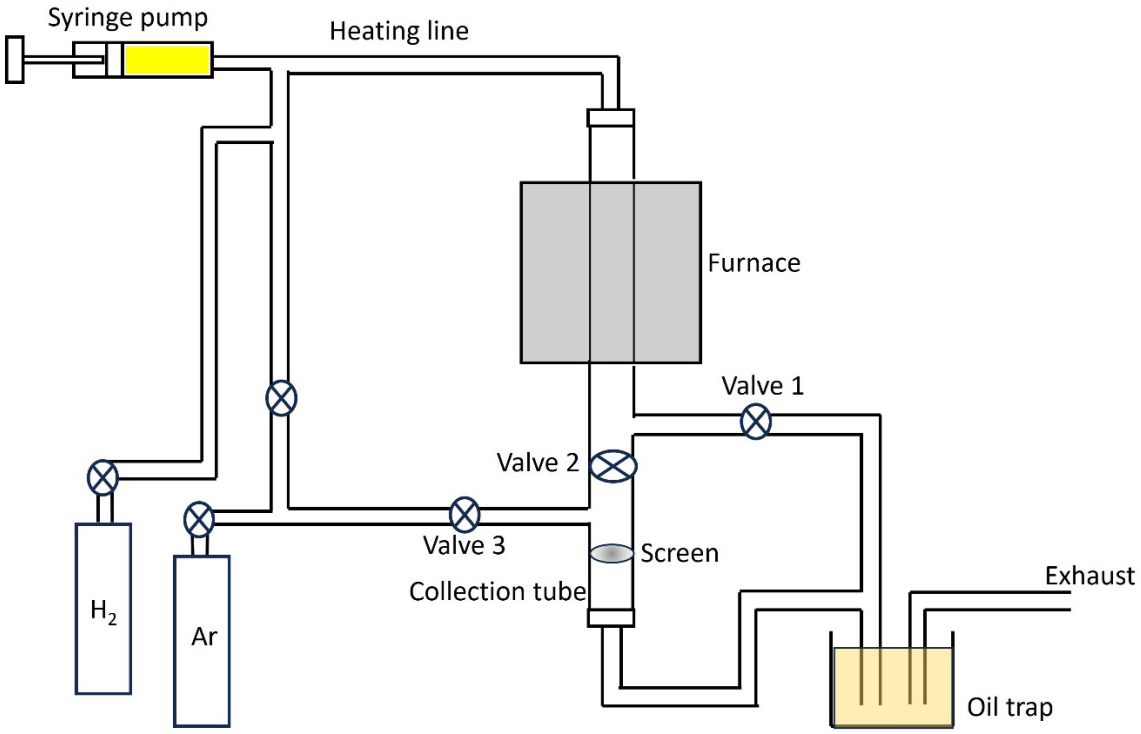

Figure 1. Schematic illustration of the FCCVD experimental setup for the SWCNT synthesis.

2.3. SWCNT Characterization

The overall morphology of CNT networks and bundles was characterized using scanning electron microscopy (SEM FS100) under 1 KV. The Energy-dispersive X-ray spectroscopy (EDS) technique was used to determine the elemental composition of the samples. Transmission electron microscopy (TEM), performed on a monochromated and aberration-corrected FEI Titan operating at 300 keV, was used to analyze the crystallinity of the CNTs, and ImageJ software was employed to determine the distance between the fringes in the bundles. Raman spectroscopy (633.8 nm He-Ne Laser and 514 nm Argon ion laser) was used to obtain the Raman spectra of SWCNTs. A UV-visible spectroscopy system (Hewlett Packard 8453) was used to obtain optical absorption spectra from SWCNT films on glass substrates. Hall effect measurement system (Ecopia HMS-5300) was employed to measure the carrier concentration, hall coefficient, sheet resistance, and carrier mobility of the synthesized SWCNT films at the temperature of T= 300K and a magnetic field of B=0.518T. Cary 670 FTIR Spectrometer was used to identify the functional groups in SWCNT thin films.

3. Results and Discussions

SWCNTs were synthesized using the FCCVD method with ferrocene ($C_{10}H_{10}Fe$) as the catalyst precursor, thiophene (C_4H_4S) as the growth promoter, ethanol (C_2H_5OH) as the carbon source, and a mixture of argon (Ar) and hydrogen (H_2) as the carrier gases with a total flow rate of 200 sccm. The growth temperature and the growth time were 1000 ^oC and 30 minutes, respectively. Fig.2(a) Shows the optical images of samples with collection times of 5, 10, 15, and 20 minutes. As the collection time increases the color of the deposited film changes from light gray to dark brown because of the increase in their thickness. Fig. 2(b) illustrates a typical SEM image of SWCNT bundles that are connected and form a continuous 2-D weblike structure [33,34]. Fig.2 (c) shows that the deposited SWCNTs mainly contain C (carbon) and Fe (iron) elements. Fe is the catalyst nanoparticle coming from the catalyst precursor ferrocene and carbon is from the SWCNTs.

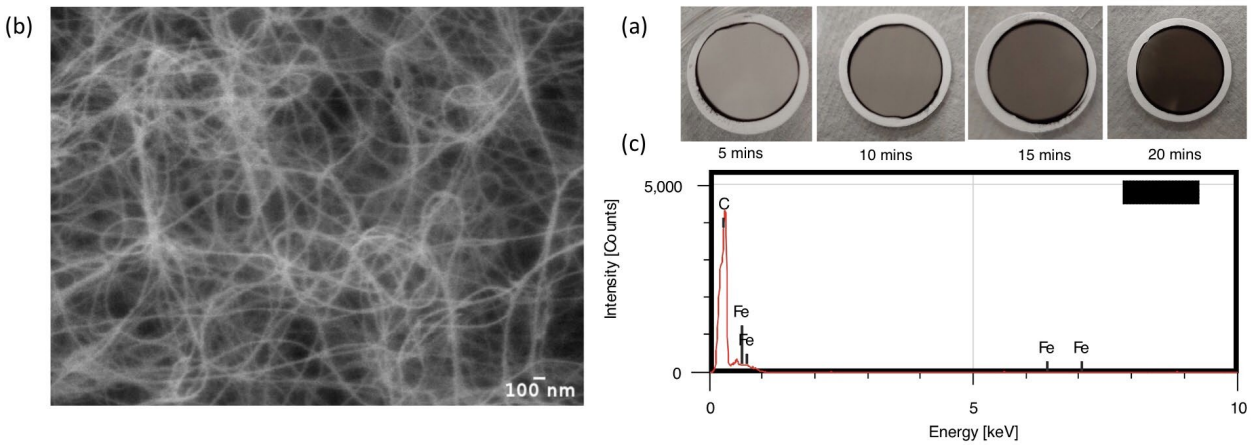

Figure 2. (a) Optical images of the samples with collection times of 5, 10, 15, and 20 minutes. (b) SEM image of SWCNT thin films. (c) EDS of the deposited SWCNTs.

Fig.3 shows the TEM images of SWCNT bundles. The morphology of the network structure of the SWCNTs and bundles can be seen in Fig.3(a). Fig.3 (b-d) are high-resolution TEM images of the SWCNTs. Using ImageJ software, the average diameter of SWCNTs in the bundles for the selected areas is measured as 1.54 nm, 1.45 nm, and 1.38 nm, respectively. The average diameter is 1.46 nm comparable with the reported values between 1-2 nm for SWCNTs' diameters [35,36,37].

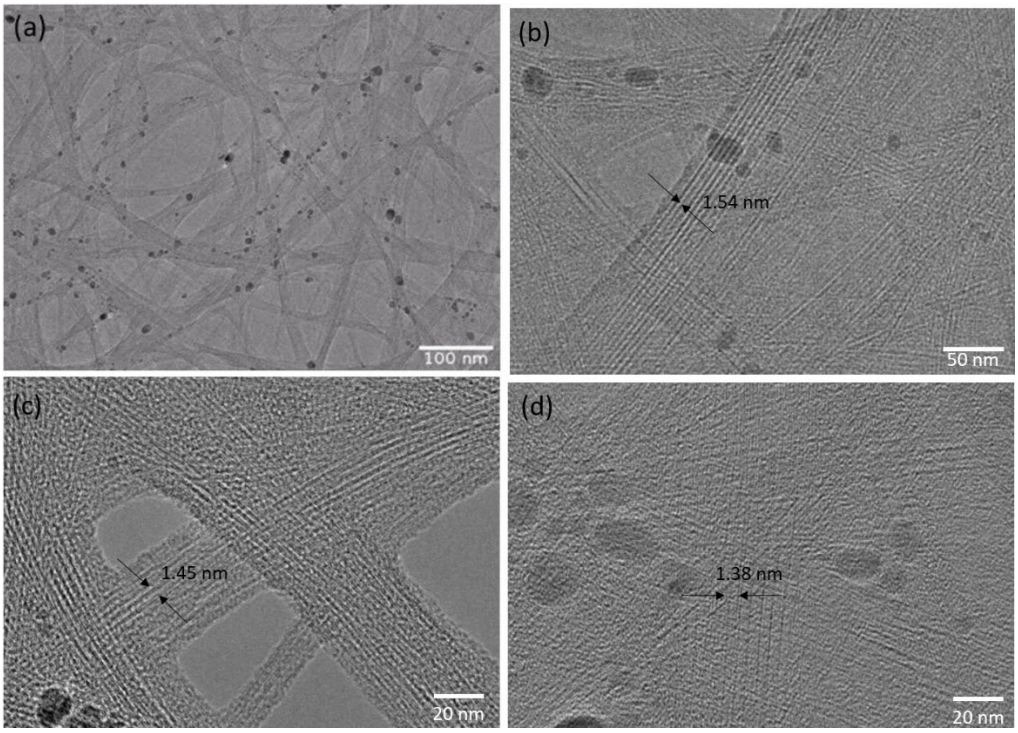

Figure 3. TEM images of deposited SWCNTs (a) The overall morphology of the SWCNTs and bundles. (b-d) different selected areas of the deposited film with the estimated average diameter of SWCNTs in the bundles as 1.54 nm, 1.45 nm, and 1.38 nm, respectively.

Raman scattering processes and specific phonon modes can identify many characteristics of SWCNTs. Examples of these specific features are carbon materials' electronic and phonon structures. Besides that, Raman spectroscopy can provide information about imperfections (defects) in SWCNTs. In general, comprehensive information about the characteristics and structure of SWCNTs can be obtained through Raman spectra because

phonons can also affect their mechanical, thermal, and elastic properties. In the Raman spectra, the intensity of the scattered light is measured as a function of its frequency downshift which can show a precise measure of the phonon frequencies in the material [38]. Fig.4 (a) shows the Raman spectra for the three samples with collection times of 10, 15, and 20 minutes employing a 633.8 nm He-Ne Laser, and Fig.4 (b) shows a zoomed image for the Raman spectra of the sample with collection time of 20 minutes using a 514 nm Argon ion laser. No peak appeared in the range of the D band indicating that our synthesized SWCNT films are highly crystallized. The emergence of a D band (usually around 1350 cm^{-1}) is related to the defects of crystalline sp^2 carbon structures [39]. Raman spectroscopy on graphene structures reveals that the D mode origin is from the edge defects [40]. The edge area in the well-crystallized SWCNTs is trivial because of the higher aspect ratio (>1000) and their atomic thickness. Therefore, they should not reveal the D band [41].

The G and G' bands at 1606 cm^{-1} and 2642 cm^{-1}, respectively, (Fig.4(a)), are comparable to the previously published values of 1585 cm^{-1} and 2700 cm^{-1} [47,37**Error! Bookmark not defined.**]. The G band specified to all the sp^2 carbon materials is related to the in-plane bond stretching mode of the C-C bonds in the hexagonal lattice [42]. G' (or 2D) band is a peak in the spectra of most sp^2 carbon materials. The origin of this peak can be ascribed to a vibrational mode identified by the breathing of six carbons related to a hexagon in the graphene lattice. By increasing the collection time no change was observed in the position of the peaks (Fig.4(a)). Because of the electron-phonon coupling or strain effect in SWCNTs, the G band splits into G^+ and G^- peaks. The split between the G^+ (at 1594 cm^{-1}) and the G^- (at 1571 cm^{-1}) picks can be seen in Fig.4(b). The G^- peak is usually unseparated from the G^+ peak, however, it can be varied in shape [43]. The signal related to the G^- peak is attributed to the SWCNT's curvature (i.e., diameter) which is specified to their electronic characteristics [44]. A small peak that appeared at 1156 cm^{-1} (Fig.4(b)) is related to the intermediate frequency modes (IFM mode). These modes which are usually reported around the range of 600-1100 cm^{-1} are considered weak and insignificant features existing in all graphene-related materials**Error! Bookmark not defined.** and are assigned to second-order, two-phonon, or one-phonon and one-elastic scattering double resonance Raman processes [45,46].

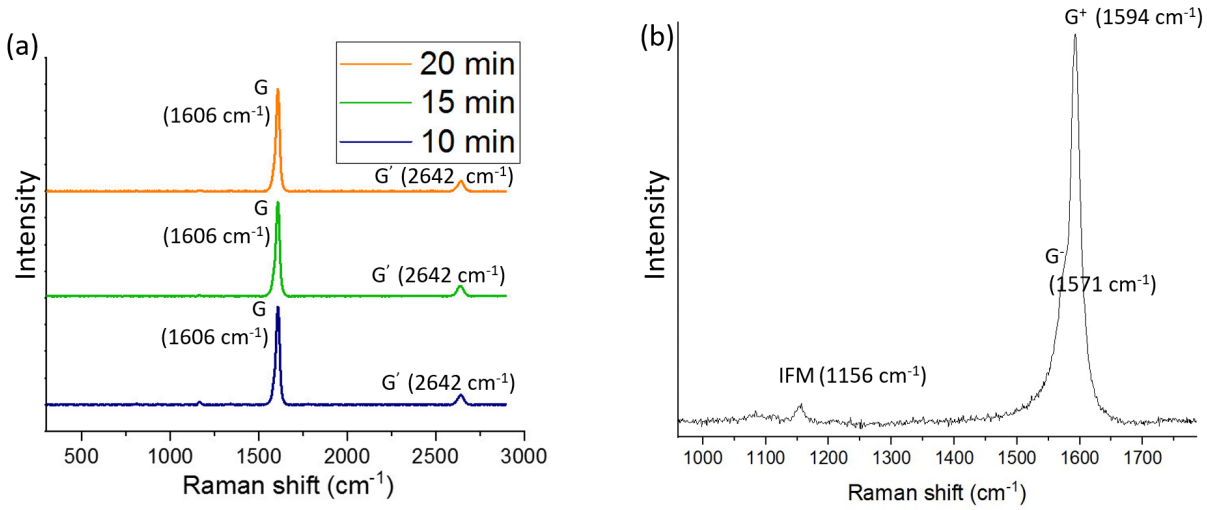

Figure 4. (a) Raman spectroscopy of the three samples with collection times of 10, 15, and 20 minutes using a 633.8 nm He-Ne Laser. (b) A zoomed image of the sample with 20 minutes of collection time using a 514 nm Argon ion laser.

Hall effect measurements are considered a precise method to determine the charge carrier density and type of the carriers in the crystalline material [47,48]. We carried out the Hall effect measurements on the SWCNT films with different collection times (5, 10, 15, 20, and 25 minutes). Important electrical properties such as carrier concentration (carrier density), mobility, Hall coefficient, and the sheet resistance of SWCNT films were explored through these measurements. The magnitudes of carrier concentration were observed between 4.6×10^{21} and 1.3×10^{23} cm^{-3}. These values are comparable to the carrier density of 10^{21}–10^{22} cm^{-3} for the purified SWCNTs synthesized through a high-pressure CO conversion process (HiPCO CNTs) or laser ablation method (LA CNTs) and chemically treated by $SOCl_2$ [31]. Compared to the values of 10^{18}–10^{19} cm^{-3} which were earlier reported for the CNT films [49] and bundles [50], our results are closer to the theoretically predicted value of ~10^{22} cm^{-3}, calculated for the aligned metallic CNTs [32]. The higher carrier density of our SWCNTs can be attributed to the advances in the synthesis method of SWCNT films and their purity [31]. For example, the dry FCCVD method allows for producing films with longer CNTs and exceptional optoelectronic properties by resolving the tradeoff between CNT length and solubility during film fabrication [19]. The mobility of the synthesized SWCNTs was in the same order of magnitude for all the collection times with an average value of ~ 0.034 cm^2/Vs. This mobility is very close to the one observed for pristine HiPCO SWCNTs (0.04 cm^2/Vs) reported by Lee et al [31]**Error! Bookmark not defined.**. The limitation factors in Hall mobility were claimed to be random networks of CNTs and barriers at inter-tube junctions of the CNT films [51,52,31].

In Fig.5 (a), the carrier concentration, Hall coefficient, and mobility are plotted versus the collection time of the SWCNT films. The carrier concentration increased from 4.6×10^{21} to 1.3×10^{23} cm^{-3} by increasing the collection time from 5 to 25 minutes while the Hall coefficient decreased from 1.35×10^{-3} to 4.6×10^{-5} (also see Table. 1). However, the decrease in mobility was trivial. Eq. 1 shows that an increase in carrier concentration will lead to a decrease in the Hall coefficient as we can see in Fig.5 (b). Also, by increasing the carrier concentration, a slight decrease was observed in the mobility of the SWCNT thin films (Fig.5 (b)). After reaching a certain value of thickness (around 800 nm for 25 minutes of collection time), the further increase did not significantly change the carrier concentration of our thin films meaning the carrier concentration became independent of the thickness. The Hall effect measurements for the samples with collection times of 5, 10, 15, 20, and 25 minutes are summarized in Table. 1. The sign of the Hall coefficients was positive for all samples showing that the synthesized SWCNTs are p-type materials.

$$R_H = 1/ne \quad (1)$$

where R_H is the Hall coefficient (cm^3/C), n is the carrier concentration (cm^{-3}), and e= 1.6×10^{-19} (C).

Figs 6(a) and 6(b) show the transmittance versus collection time and sheet resistance. By increasing the collection time from 5 to 25 minutes, the transmittance and sheet resistance of the samples decreased from 95 % to 43 % and 370 to 21 ohm/square, respectively. Increasing the collection time leads to an increase in the thickness of the thin films, which will lead to a decrease in the sheet resistance of the materials as indicated by Eq. 2. The observed sheet resistance and transmittance magnitudes are comparable with the ones reported for the SWCNT thin films [30,35,53].

$$R_s = p/t \quad (2)$$

where R_s is the sheet resistance (ohm/square), p is resistivity (ohm.cm), and t is the thickness of the thin film (cm).

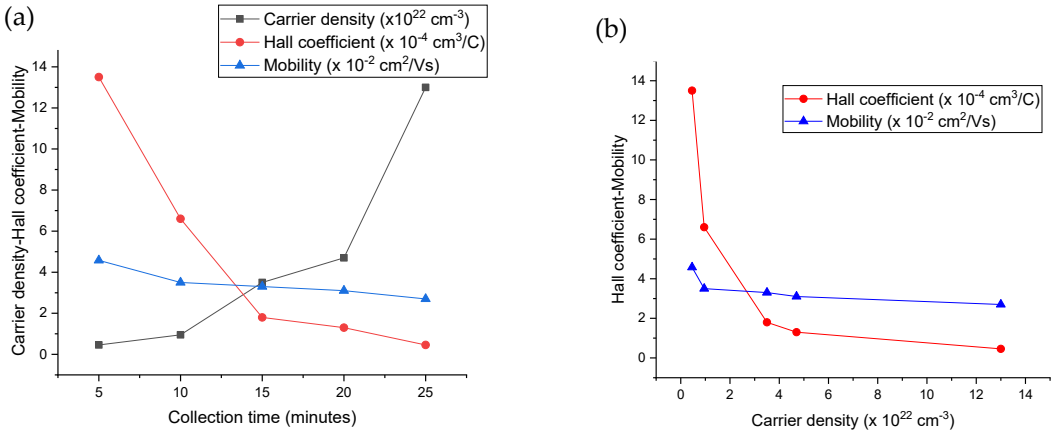

Figure 5. Graphs of (a) carrier density, Hall coefficient, and mobility versus collection time of SWCNT films and, (b) Hall coefficient and mobility versus carrier density.

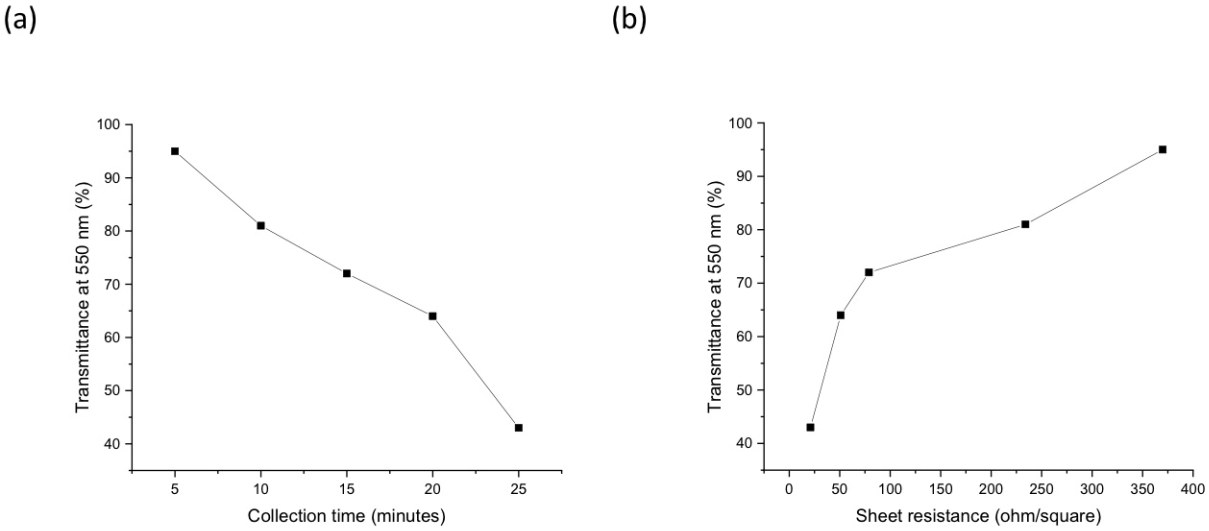

Figure 6. Graphs of transmittance versus (a) collection time and (b) sheet resistance.

Table 1. Hall effect measurements for the samples with collection times of 5, 10, 15, 20, and 25 minutes.

Carrier density (cm^{-3})	Mobility (cm^2/Vs)	Hall coefficient (cm^3/C)	Carrier type	Sheet resistance (ohm/square)	Collection time (minutes)
$4.6x10^{21}$	$4.58x10^{-2}$	1.35×10^{-3}	P-type	370	5
$9.5x10^{21}$	$3.5x10^{-2}$	$6.6x10^{-4}$	P-type	234	10
3.5×10^{22}	3.3×10^{-2}	1.8×10^{-4}	P-type	79	15
4.7×10^{22}	3.1×10^{-2}	1.3×10^{-4}	P-type	51	20
1.3×10^{23}	2.7×10^{-2}	4.6×10^{-5}	P-type	21	25

Controlling the electronic properties of CNTs can develop their technical applications in different fields. Transferring charges (electrons or holes) to the nanotube through intercalation and/or functionalization processes is one way to change the carbon nanotube's electronic and vibrational characteristics [54,55,56]. Therefore, it is important to study the effect of doping on CNTs' electrical properties.

Different acid treatments were done on the SWCNT films with the same collection time to investigate the effect of doping on their electrical properties. The conclusion obtained from treating one sample can be applied to the samples with different collection times. The samples with 10 minutes of collection time (transmittance of 80%) were treated with sulfuric, nitric, and hydrochloric acids with different acid concentrations (Table. 2). All the samples were rinsed with deionized (DI) water after being treated with acids while in some cases (Case C in Table. 2) the samples were first rinsed with ethanol followed by DI water. In Case B, the samples were heated at 80 ^{o}C during the time of the treatment (30 minutes). The Hall effect measurements were applied to the samples after the treatments to study the change in their electrical characteristics.

All the samples maintained their p-type characteristic after being treated with acids. Acceptor-type doping of the SWCNTs was observed by other researchers using Brønsted acids (like sulfuric, nitric, and hydrochloric acid) [28,57,58,59]. Compared to the sample without any treatment (Case G), the hole mobility increased in all acid-treated samples, the hole concentration of all sulfuric acid and hydrochloric acid treated samples decreased, but the hole concentration of the nitric acid-treated sample increased. Experimental results showed that nitric acid treatment can improve the SWCNT film's mobility and carrier concentration (Case F). The corresponding conductivity was calculated for the samples using Eq. 3.

$$\sigma=\mu ne \quad (3)$$

Here σ is the conductivity due to holes in a unit of Siemens per meter (S/m) or $\Omega^{-1}m^{-1}$, n and e stand for electronic carrier concentration and electron charge respectively, and μ is hole mobility.

Despite a slight decrease in hole concentration, the conductivity increased in all kinds of acid treatments while the sheet resistance decreased as can be seen in Table. 2. Although the sample treated with sulfuric acid at 80°C (Case B) showed the highest hole mobility, the highest conductivity (30720 S/m) is related to the nitric acid treatment (Case F). Additionally, there was a significant decrease in sheet resistance of the nitric acid-treated sample (Case F) to 43 ohm/square compared to the untreated sample with a sheet resistance of 243 ohm/square (Case G). The second and third highest conductivity are 14060 S/m and 12096 S/m for the films with the hydrochloric acid treatment and DI water rinsing (Case E) and the sulfuric acid treatment with ethanol as well as DI water rinsing (Case C), respectively. All the calculated conductivities were in the reported range (on the order of 10^2 to 10^6 S/cm) for SWCNT [60]. Improvement in the conductivity of the SWCNT films can be related to the downshifts in the Fermi level toward valence bands of SWCNTs leading to the reduction in the Schottky barrier height and increasing the conductivity of the films [61,30].

The bar graphs (Fig. 7) show the comparison between the electrical properties of SWCNT thin films under different acid treatments according to the data in Table. 2. Overall, we can see the enhancement in the electrical properties of SWCNT films after the acid treatments with the increase in hole mobility and conductivity as well as the decrease in the sheet resistance in all cases. Out of all the samples, the ones treated with sulfuric acid at a temperature of 80°C (Case B) showed the greatest hole mobility of 1.5 cm^2/Vs (Figure 7(b)). However, the sample treated with nitric acid (Case F) demonstrated the highest carrier conductivity of 30720 S/m (Figure 7(e)), the highest carrier density of 1.2 x 10^{22} cm^{-3} (Figure 7(a)), and the lowest sheet resistance of 43 ohm/square (Figure 7(d)).

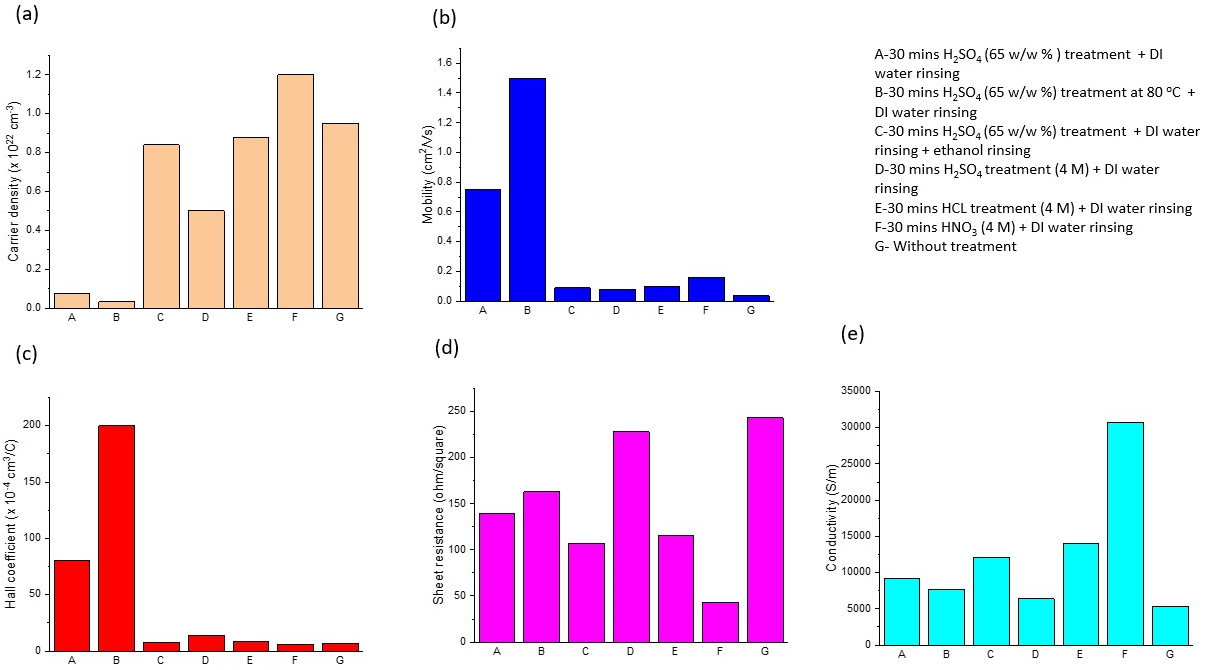

Figure 7. Bar graphs showing the effect of different acid treatments on (a) carrier density, (b) hole mobility, (c) Hall coefficient, (d) sheet resistance, and (e) conductivity of the SWCNT thin films.

Fourier Transform Infrared Spectroscopy (FTIR) was utilized to analyze the chemical structure of sulfuric acid-treated SWCNTs at 80°C (Case B) and nitric acid-treated SWCNTs (Case F) in comparison to pristine SWCNTs (Case G). The analysis was conducted by identifying functional groups and comparing any changes observed in the three cases. Fig.8 shows FTIR of pristine SWCNTs (Case G), HNO_3-treated SWCNTs (Case F), and H_2SO_4-treated SWCNTs heated at 80°C (Case B) in the wavelength ranges of 500-1600 cm^{-1} (Fig.8(a)) and 1600-4000 cm^{-1} (Fig.8(b)). The peaks at 630, 701, 719, 797, 837, and 1010 cm^{-1} in all three samples are related to the C=C bending of the alkene functional group [62,63], while the peak at 872 cm^{-1} comes from the bending of the C-H for the benzene derivative functional group [64]. Hydrogen exists in the precursor solution for the synthesis of SWCNTs and is also used as a carrier gas during the synthesis process. A new peak appeared at 1046 cm^{-1} for the sulfuric acid-treated sample, which represents the S=O stretching of sulfoxide [65] and is attributed to the sulfuric acid treatment. The peaks at 1073, 1106, 1153, 1244, and 1297 cm^{-1}, common in all three samples, are related to the C-O stretching mode of the primary alcohol, secondary alcohol, tertiary alcohol, and alkyl aryl ether functional groups [62,66]. Ethanol is a primary alcohol that is used in the precursor solution. Secondary and tertiary alcohols can form by attaching the hydroxyl group (-OH) to a carbon atom that is bonded to two and three alkyl groups (or hydrocarbon chains) respectively [67]. Ether is formed when an oxygen atom is attached to two alkyl or aryl groups (aromatic hydrocarbons) [68]. For all samples, the peak at 1322 cm^{-1} represents the S=O stretching mode of the sulfone, and the peak at 1409 cm^{-1} is related to the S=O stretching mode of the sulfate functional group [69,62**Error! Bookmark not defined.**]. Sulfur comes from thiophene which is used in the precursor solution.

The 1488 and 1578 cm^{-1} peaks appearing in all three samples originate from the C-H bending of alkane and the C=C stretching of cyclic alkane functional groups, respectively [70]. The peak at 1735 cm^{-1} for pristine and nitric acid-treated SWCNTs corresponds to the C=O stretching mode in carbonyl or carboxylic acid groups [71]. This peak (1735 cm^{-1}) is downshifted to 1633 cm^{-1} for the sulfuric acid-treated sample representing the C=C stretching of alkene [72]. This change in wavelength may be related to increased energy from heating, leading to an increase in frequency and a decrease in the wavelength. The sulfuric

acid-treated sample also shows a new peak at 2113 cm^{-1} related to the C≡C stretching of the alkyne functional group. This peak can be compared to the one at 1909 cm^{-1} for the pristine SWCNT sample showing the C=C=C stretching of the allene functional group [62]. This change in the bond formation from double-bond carbon in the pristine SWCNTs into triple-bond in the sulfuric acid-treated sample can also be attributed to the heating during the acid treatment. Wong et al. [73] conducted simulations on the distribution of chemical bonds in carbon chains. Their findings suggest that as the temperature rises, carbon atoms in a compound may transition from a double bond to a single or triple bond. This transition is dependent on energy minimization and the Octet rule. The Octet rule dictates that an atom's valence shell can only accommodate a maximum of eight electrons and no lone pair electrons are permitted.

In the range of 1600-4000 cm^{-1}, two new peaks appeared at 2031 and 2169 cm^{-1} for the nitric acid-treated sample. These peaks can be related to N=C=S stretching of isothiocyanate and S-C≡N stretching of thiocyanate, respectively [62]. Sulfur exists in the precursor solution coming from thiophene. The peaks at 3092 and 3647 cm^{-1} appeared for pristine and nitric acid-treated SWCNTs corresponding to the O-H stretching of alcohol (hydroxyl functional group). The peak at 3382 cm^{-1} for the sulfuric acid-treated sample is also related to the O-H stretching of alcohol [74]. These peaks are usually broad and strong in the 3200-3550 cm^{-1} range [62], as seen in Fig.8 (b). The disappearance of one of the peaks related to O-H stretching and also the peak related to C=O stretching (at 1735 cm^{-1}) for the sulfuric acid-treated sample might be a reason for the increase in the hole mobility of this sample. Studies have shown that polar groups such as hydroxyl and carbonyl functional groups can form deep traps that can capture electric charge carrier [75,76]. Scattering and capture of free charges by deep traps can lead to the energy loss of the charge carriers and a decrease in their mobility [76]. Therefore, the reduction in the number of polar groups such as carbonyl and hydroxyl functional groups in the sulfuric acid-treated sample might play a role in improving its mobility. Compared to the sulfuric acid-treated sample, the FTIR spectra of the nitric acid-treated one are more similar to the pristine SWCNTs' spectra. However, the improved electrical properties of the nitric acid-treated SWCNTs might be related to the existence of two new picks (2031 and 2169 cm^{-1}) in this sample representing the isothiocyanate and thiocyanate functional groups. Polymers containing thiocyanate have been widely reported to be used as hole-transporting layers in optoelectronic applications (such as solar cells) due to the improvement in the charge extraction efficiency related to increased conductivity [77,78].

In summary, among the different acid treatments, the sample treated with sulfuric acid at a temperature of 80°C (Case B) exhibited the highest hole mobility value of 1.5 cm^2/Vs. And, the sample treated with nitric acid (Case F) demonstrated the highest carrier conductivity of 30720 S/m, the highest carrier density of 1.2×10^{22} cm^{-3}, and the lowest sheet resistance of 43 ohm/square. These improvements in the electrical properties of both samples make them suitable for electronic applications such as thin film transistors or solar cells.

Table 2. Hall effect measurements of the SWCNT film of collection time of 10 minutes after acid treatments.

Case	Acid treatment	Carrier density (cm^{-3})	Hole Mobility (cm^2/Vs)	Hall coefficient (cm^3/C)	Carrier type	Sheet resistance (ohm/square)	Conductivity (S/m)
A	30 mins H_2SO_4 (65 w/w %) treatment + DI water rinsing	7.7×10^{20}	0.75	8×10^{-3}	P-type	139	9240
B	30 mins H_2SO_4 (65 w/w %) treatment at 80 ^oC + DI water rinsing	3.2×10^{20}	1.5	2×0^{-2}	P-type	163	7680
C	30 mins H_2SO_4 (65 w/w %) treatment + DI water rinsing + ethanol rinsing	8.4×10^{21}	0.09	7.7×10^{-4}	P-type	107	12096
D	30 mins H_2SO_4 treatment (4 M) + DI water rinsing	5×10^{21}	0.08	1.4×10^{-3}	P--type	228	6400
E	30 mins HCL treatment (4 M) + DI water rinsing	8.8×10^{21}	0.1	8.8×10^{-4}	P-type	115	14060
F	30 mins HNO_3 (4 M) + DI water rinsing	1.2×10^{22}	0.16	5.8×10^{-4}	P-type	43	30720
G	Without treatment	9.5×10^{21}	0.035	6.6×10^{-4}	P-type	243	5320

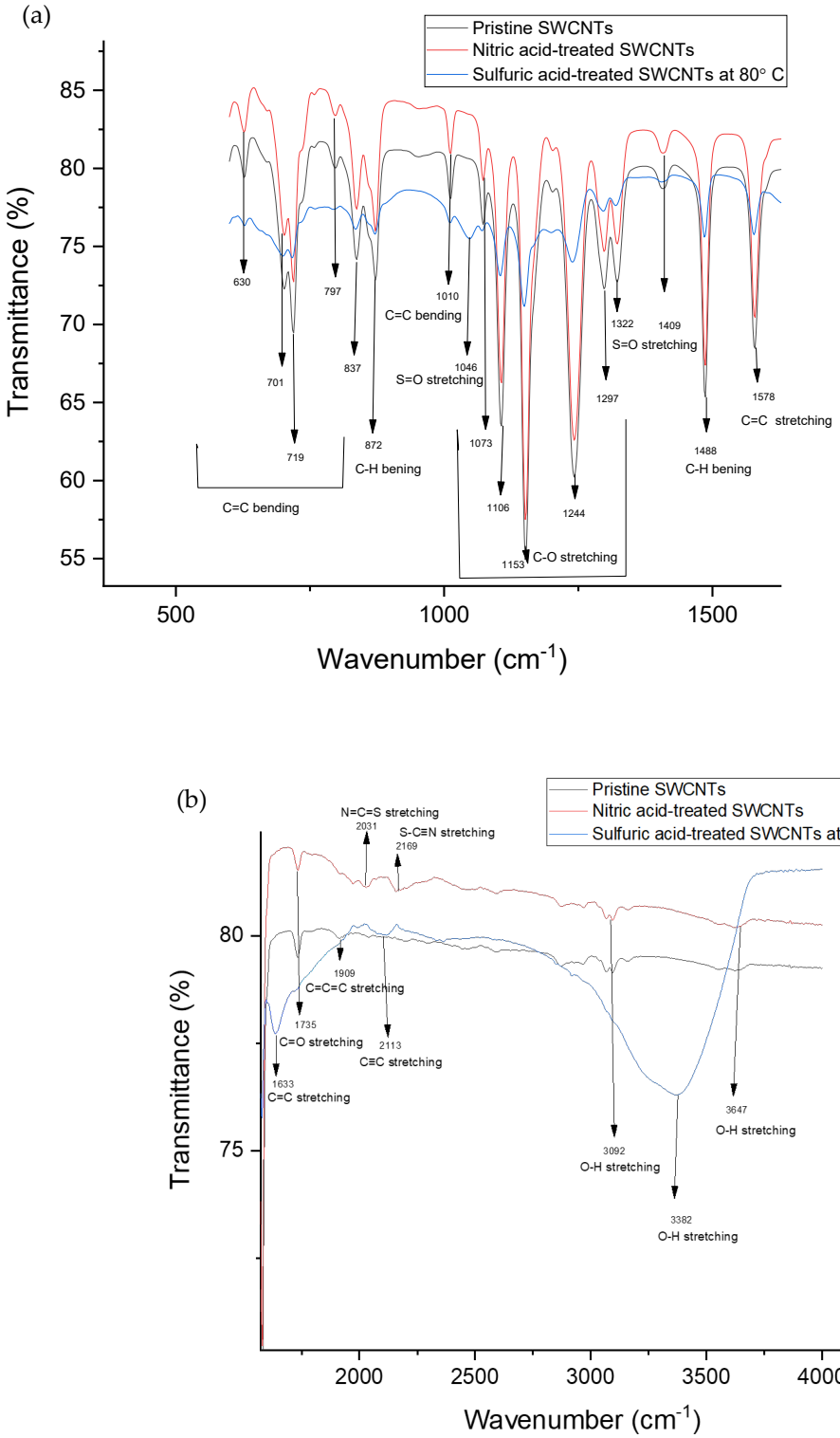

Figure 8. FTIR spectra of pristine SWCNTs, HNO_3-treated SWCNTs, and H_2SO_4-treated SWCNTs heated at 80°C in the wavelength ranges of (a) 500-1600 cm^{-1} and (b) 1600-4000 cm^{-1}.

4. Conclusion

High-yield SWCNT films were synthesized through a floating catalyst chemical vapor deposition method using a low flow rate of 200 sccm as the total flow rate of the mixed argon and hydrogen gases. The structural properties of the thin films were investigated

by SEM, TEM, FTIR and Raman spectroscopy. The Raman spectra of the synthesized SWCNTs showed no peak in the range of the D-band confirming that the SWCNT films are highly crystallized. Significant electrical characteristics of the SWCNT films such as carrier concentration, carrier mobility, Hall coefficient, and sheet resistance were investigated through the Hall effect measurements. The samples showed a high carrier concentration of 10^{21}-10^{23} cm^{-3} with the transmittance between 95-43%. The effect of different acid treatments was explored using nitric, sulfuric, and hydrochloric acids. In all the treatments, an increase was observed in carrier mobility and conductivity while their sheet resistance decreased. The samples remained p-type after the acid treatments showing that the treatments led to the p doing. Samples treated with sulfuric acid at 80 ^{o}C showed the highest mobility of 1.5 cm^2/Vs. On the other hand, the highest carrier conductivity (30720 S/m) and the lowest sheet resistance (43 ohm/square) were obtained from the samples treated with nitric acids. The presence of multiple functional groups in our synthesized SWCNTs may increase their potential for various applications since each functional group exhibits distinct characteristics and reactivity, enabling participation in various types of reactions and increasing functionality. Improving the electrical properties of SWCNTs can lead to a great enhancement in their electronic applications. Since the synthesized SWCNT films maintained their p-type nature after the acid treatments, the enhancement in their electrical characteristics makes them suitable candidates for hole-transporting layers in solar cells.

Acknowledgments: This work was supported by the National Science Foundation under grants 1506640, 2134375, and 2213923. This work was performed, in part, at the Center for Integrated Nanotechnologies, an Office of Science User Facility operated for the U.S. Department of Energy (DOE) Office of Science. Los Alamos National Laboratory, an affirmative action equal opportunity employer, is managed by Triad National Security, LLC for the U.S. Department of Energy's NNSA, under contract 89233218CNA000001. We thank Prof. Jin He, Dr. Govinda Ghimire, and Dr. Vadym Drozd (FIU CESMEC) for the help with the Raman measurements, Prof. Indranil Chakraborty and FIU Chemistry Department for the FTIR measurements, and Prof. Christopher Dares and Dr. Xiangyang Hou for the UV-Vis measurements. The authors would also like to acknowledge the support from the Advanced Materials Engineering Research Institutes (AMERI) at Florida International University.

Data Availability: The raw data required to reproduce these findings are available by request from the corresponding author. The Processed data required to reproduce these findings are available by request from the corresponding author.

References

1. Maruyama, T. (2021). Carbon nanotubes. In Handbook of Carbon-Based Nanomaterials (pp. 299-319). Elsevier.
2. Dresselhaus, M. S., & Avouris, P. (2001). Introduction to carbon materials research. In Carbon nanotubes: synthesis, structure, properties, and applications (pp. 1-9). Berlin, Heidelberg: Springer Berlin Heidelberg.
3. Iijima, S. (1991). Helical microtubules of graphitic carbon. nature, 354(6348), 56-58.
4. Iijima, S., & Ichihashi, T. (1993). Single-shell carbon nanotubes of 1-nm diameter. nature, 363(6430), 603-605.
5. Wu, K., Niu, Y., Zhang, Y., Yong, Z., & Li, Q. (2021). Continuous growth of carbon nanotube films: From controllable synthesis to real applications. Composites Part A: Applied Science and Manufacturing, 144, 106359.
6. Di, J., Wang, X., Xing, Y., Zhang, Y., Zhang, X., Lu, W., ... & Zhu, Y. T. (2014). Dry-Processable Carbon Nanotubes for Functional Devices and Composites. Small, 10(22), 4606-4625.
7. Liu, L., Ma, W., & Zhang, Z. (2011). Macroscopic carbon nanotube assemblies: preparation, properties, and potential applications. Small, 7(11), 1504-1520.
8. Peng, B., Locascio, M., Zapol, P., Li, S., Mielke, S. L., Schatz, G. C., & Espinosa, H. D. (2008). Measurements of near-ultimate strength for multiwalled carbon nanotubes and irradiation-induced crosslinking improvements. Nature nanotechnology, 3(10), 626-631.
9. Bai, Y., Zhang, R., Ye, X., Zhu, Z., Xie, H., Shen, B., ... & Wei, F. (2018). Carbon nanotube bundles with tensile strength over 80 GPa. Nature nanotechnology, 13(7), 589-595.
10. Chen, H., Zeng, S., Chen, M., Zhang, Y., & Li, Q. (2015). Fabrication and functionalization of carbon nanotube films for high-performance flexible supercapacitors. Carbon, 92, 271-296.
11. Zhou, Y., & Azumi, R. (2016). Carbon nanotube based transparent conductive films: progress, challenges, and perspectives. Science and Technology of advanced MaTerialS, 17(1), 493-516.

12. Liao, Y., Hussain, A., Laiho, P., Zhang, Q., Tian, Y., Wei, N., ... & Kauppinen, E. I. (2018). Tuning Geometry of SWCNTs by CO2 in Floating Catalyst CVD for High-Performance Transparent Conductive Films. Advanced Materials Interfaces, 5(23), 1801209.
13. Meysami, S. S., Koos, A. A., Dillon, F., & Grobert, N. (2013). Aerosol-assisted chemical vapour deposition synthesis of multi-wall carbon nanotubes: II. An analytical study. Carbon, 58, 159-169
14. Choi, Y. C., Bae, D. J., Lee, Y. H., Lee, B. S., Park, G. S., Choi, W. B., ... & Kim, J. M. (2000). Growth of carbon nanotubes by microwave plasma-enhanced chemical vapor deposition at low temperature. Journal of Vacuum Science & Technology A: Vacuum, Surfaces, and Films, 18(4), 1864-1868.
15. Makris, T. D., Giorgi, R., Lisi, N., Pilloni, L., Salernitano, E., Sarto, F., & Alvisi, M. (2004). Carbon nanotubes growth by HFCVD: effect of the process parameters and catalyst preparation. Diamond and Related Materials, 13(2), 305-310.
16. Byon, H. R., Lim, H. S., Song, H. J., & Choi, H. C. (2007). A synthesis of high purity single-walled carbon nanotubes from small diameters of cobalt nanoparticles by using oxygen-assisted chemical vapor deposition process. Bulletin of the Korean Chemical Society, 28(11), 2056-2060.
17. Feng, C., Liu, K., Wu, J. S., Liu, L., Cheng, J. S., Zhang, Y., ... & Jiang, K. (2010). Flexible, stretchable, transparent conducting films made from superaligned carbon nanotubes. Advanced Functional Materials, 20(6), 885-891.
18. Bronikowski, M. J., Willis, P. A., Colbert, D. T., Smith, K. A., & Smalley, R. E. (2001). Gas-phase production of carbon single-walled nanotubes from carbon monoxide via the HiPco process: A parametric study. Journal of Vacuum Science & Technology A: Vacuum, Surfaces, and Films, 19(4), 1800-1805.
19. Zhang, Q., Wei, N., Laiho, P., & Kauppinen, E. I. (2019). Recent developments in single-walled carbon nanotube thin films fabricated by dry floating catalyst chemical vapor deposition. Single-Walled Carbon Nanotubes: Preparation, Properties and Applications, 99-128.
20. Bogdanova, A. R., Krasnikov, D. V., & Nasibulin, A. G. (2023). The role of sulfur in the CVD carbon nanotube synthesis. Carbon, 118051.
21. Chen, D. R., Chitranshi, M., Schulz, M., & Shanov, V. (2019). A review of three major factors controlling carbon nanotubes synthesis from the floating catalyst chemical vapor deposition. Nano Life, 9(04), 1930002.
22. Yu, F., Yang, M., Li, F., Su, C., Ma, B., Yuan, Z., ... & Ma, J. (2012). The growth mechanism of single-walled carbon nanotubes with a controlled diameter. Physica E: Low-dimensional Systems and Nanostructures, 44(10), 2032-2040.
23. Plata, D. L., Meshot, E. R., Reddy, C. M., Hart, A. J., & Gschwend, P. M. (2010). Multiple alkynes react with ethylene to enhance carbon nanotube synthesis, suggesting a polymerization-like formation mechanism. Acs Nano, 4(12), 7185-7192.
24. Chen, D. R., Chitranshi, M., Schulz, M., & Shanov, V. (2019). A review of three major factors controlling carbon nanotubes synthesis from the floating catalyst chemical vapor deposition. Nano Life, 9(04), 1930002.
25. Huang, S., Cai, Q., Chen, J., Qian, Y., & Zhang, L. (2009). Metal-catalyst-free growth of single-walled carbon nanotubes on substrates. Journal of the American Chemical Society, 131(6), 2094-2095.
26. Li, Y., Ji, K., Duan, Y., Meng, G., & Dai, Z. (2017). Effect of hydrogen concentration on the growth of carbon nanotube arrays for gecko-inspired adhesive applications. Coatings, 7(12), 221.
27. Ma, Y., Dichiara, A. B., He, D., Zimmer, L., & Bai, J. (2016). Control of product nature and morphology by adjusting the hydrogen content in a continuous chemical vapor deposition process for carbon nanotube synthesis. Carbon, 107, 171-179.
28. Graupner, R., Abraham, J., Vencelová, A., Seyller, T., Hennrich, F., Kappes, M. M., ... & Ley, L. (2003). Doping of single-walled carbon nanotube bundles by Brønsted acids. Physical Chemistry Chemical Physics, 5(24), 5472-5476.
29. Dresselhaus, M. S., & Dresselhaus, G. (1981). Intercalation compounds of graphite. Advances in Physics, 30(2), 139-326.
30. Ding, E. X., Jiang, H., Zhang, Q., Tian, Y., Laiho, P., Hussain, A., ... & Kauppinen, E. I. (2017). Highly conductive and transparent single-walled carbon nanotube thin films from ethanol by floating catalyst chemical vapor deposition. Nanoscale, 9(44), 17601-17609.
31. Lee, S. H., Uhm, T. W., You, Y. G., Kim, S. W., Jhang, S. H., Dettlaff-Weglikowska, U., & Park, Y. W. (2014). Hall effect in carbon nanotube thin films. Synthetic metals, 198, 84-87.
32. Mintmire, J. W., Dunlap, B. I., & White, C. T. (1992). Are fullerene tubules metallic?. Physical review letters, 68(5), 631.
33. Niu, Z., Zhou, W., Chen, J., Feng, G., Li, H., Ma, W., ... & Xie, S. (2011). Compact-designed supercapacitors using free-standing single-walled carbon nanotube films. Energy & Environmental Science, 4(4), 1440-1446.
34. Ma, W., Song, L., Yang, R., Zhang, T., Zhao, Y., Sun, L., ... & Xie, S. (2007). Directly synthesized strong, highly conducting, transparent single-walled carbon nanotube films. Nano Letters, 7(8), 2307-2311.
35. Hussain, A., Liao, Y., Zhang, Q., Ding, E. X., Laiho, P., Ahmad, S., ... & Kauppinen, E. I. (2018). Floating catalyst CVD synthesis of single walled carbon nanotubes from ethylene for high performance transparent electrodes. Nanoscale, 10(20), 9752-9759.
36. Ajayan, P. M., & Ebbesen, T. W. (1997). Nanometre-size tubes of carbon. Reports on Progress in Physics, 60(10), 1025.
37. Ruoff, R. S., Qian, D., & Liu, W. K. (2003). Mechanical properties of carbon nanotubes: theoretical predictions and experimental measurements. Comptes Rendus Physique, 4(9), 993-1008.
38. Dresselhaus, M. S., Dresselhaus, G., Saito, R., & Jorio, A. (2005). Raman spectroscopy of carbon nanotubes. Physics reports, 409(2), 47-99.
39. Pimenta, M. A., Dresselhaus, G., Dresselhaus, M. S., Cancado, L. G., Jorio, A., & Saito, R. (2007). Studying disorder in graphite-based systems by Raman spectroscopy. Physical chemistry chemical physics, 9(11), 1276-1290.
40. Ferrari, A. C., Meyer, J. C., Scardaci, V., Casiraghi, C., Lazzeri, M., Mauri, F., ... & Geim, A. K. (2006). Raman spectrum of graphene and graphene layers. Physical review letters, 97(18), 187401.

41. Park, Y., Hembram, K. P. S. S., Yoo, R., Jang, B., Lee, W., Lee, S. G., ... & Lee, J. K. (2019). Reinterpretation of single-wall carbon nanotubes by Raman spectroscopy. The Journal of Physical Chemistry C, 123(22), 14003-14009.
42. Jorio, A., & Saito, R. (2021). Raman spectroscopy for carbon nanotube applications. Journal of Applied Physics, 129(2), 021102.
43. Jorio, A., Souza Filho, A. G., Dresselhaus, G., Dresselhaus, M. S., Swan, A. K., Ünlü, M. S., ... & Saito, R. (2002). G-band resonant Raman study of 62 isolated single-wall carbon nanotubes. Physical Review B, 65(15), 155412.
44. Kataura, H., Kumazawa, Y., Maniwa, Y., Umezu, I., Suzuki, S., Ohtsuka, Y., & Achiba, Y. (1999). Optical properties of single-wall carbon nanotubes. Synthetic metals, 103(1-3), 2555-2558.
45. Saito, R., Jorio, A., Souza Filho, A. G., Dresselhaus, G., Dresselhaus, M. S., & Pimenta, M. A. (2001). Probing phonon dispersion relations of graphite by double resonance Raman scattering. Physical review letters, 88(2), 027401.
46. Saito, R., Grüneis, A., Samsonidze, G. G., Brar, V. W., Dresselhaus, G., Dresselhaus, M. S., ... & Souza Filho, A. G. (2003). Double resonance Raman spectroscopy of single-wall carbon nanotubes. New Journal of Physics, 5(1), 157.
47. Yomogida, Y., Horiuchi, K., Okada, R., Kawai, H., Ichinose, Y., Nishidome, H., ... & Yanagi, K. (2022). Hall effect in gated single-wall carbon nanotube films. Scientific Reports, 12(1), 101.
48. Hall, E. H. (1879). On a new action of the magnet on electric currents. American Journal of Mathematics, 2(3), 287-292.
49. Baumgartner, G., Carrard, M., Zuppiroli, L., Bacsa, W., de Heer, W. A., & Forró, L. (1997). Hall effect and magnetoresistance of carbon nanotube films. Physical Review B, 55(11), 6704.
50. Song, S. N., Wang, X. K., Chang, R. P. H., & Ketterson, J. B. (1994). Electronic properties of graphite nanotubules from galvanomagnetic effects. Physical Review Letters, 72(5), 697.
51. Martel, R., Schmidt, T., Shea, H. R., Hertel, T., & Avouris, P. (1998). Single-and multi-wall carbon nanotube field-effect transistors. Applied physics letters, 73(17), 2447-2449.
52. Dürkop, T., Getty, S. A., Cobas, E., & Fuhrer, M. S. (2004). Extraordinary mobility in semiconducting carbon nanotubes. Nano letters, 4(1), 35-39.
53. Kaskela, A., Laiho, P., Fukaya, N., Mustonen, K., Susi, T., Jiang, H., ... & Kauppinen, E. I. (2016). Highly individual SWCNTs for high performance thin film electronics. Carbon, 103, 228-234.
54. Barros, E. B., Son, H., Samsonidze, G. G., Souza Filho, A. G., Saito, R., Kim, Y. A., ... & Dresselhaus, M. S. (2007). Raman spectroscopy of double-walled carbon nanotubes treated with H 2 S O 4. Physical Review B, 76(4), 045425.
55. Rao, A. M., Eklund, P. C., Bandow, S., Thess, A., & Smalley, R. E. (1997). Evidence for charge transfer in doped carbon nanotube bundles from Raman scattering. Nature, 388(6639), 257-259.
56. Fagan, S. B., Souza Filho, A. G. D., Mendes Filho, J., Corio, P., & Dresselhaus, M. S. (2005). Electronic properties of Ag-and CrO3-filled single-wall carbon nanotubes. Chemical Physics Letters, 406(1-3), 54-59.
57. Wang, P. C., Liao, Y. C., Lai, Y. L., Lin, Y. C., Su, C. Y., Tsai, C. H., & Hsu, Y. J. (2012). Conversion of pristine and p-doped sulfuric-acid-treated single-walled carbon nanotubes to n-type materials by a facile hydrazine vapor exposure process. Materials Chemistry and Physics, 134(1), 325-332.
58. Hennrich, F., Wellmann, R., Malik, S., Lebedkin, S., & Kappes, M. M. (2003). Reversible modification of the absorption properties of single-walled carbon nanotube thin films via nitric acid exposure. Physical Chemistry Chemical Physics, 5(1), 178-183.
59. Sumanasekera, G. U., Allen, J. L., Fang, S. L., Loper, A. L., Rao, A. M., & Eklund, P. C. (1999). Electrochemical oxidation of single wall carbon nanotube bundles in sulfuric acid. The Journal of Physical Chemistry B, 103(21), 4292-4297.
60. Earp, B., Dunn, D., Phillips, J., Agrawal, R., Ansell, T., Aceves, P., ... & Luhrs, C. (2020). Enhancement of electrical conductivity of carbon nanotube sheets through copper addition using reduction expansion synthesis. Materials Research Bulletin, 131, 110969.
61.
1. Kim, K. K., Bae, J. J., Park, H. K., Kim, S. M., Geng, H. Z., Park, K. A., ... & Lee, Y. H. (2008). Fermi level engineering of single-walled carbon nanotubes by AuCl3 doping. Journal of the American Chemical Society, 130(38), 12757-12761.
62. Sigma, M. (2022). IR Spectrum Table & Chart. Repéré le, 03-6.
63. Kamble, R. V., Bhinge, S. D., Mohite, S. K., Randive, D. S., & Bhutkar, M. A. (2021). In vitro targeting and selective killing of mcf-7 and colo320dm cells by 5-fluorouracil anchored to carboxylated SWCNTs and MWCNTs. Journal of Materials Science: Materials in Medicine, 32(6), 71.
64. Klein, D. R. (2022). Organic Chemistry. John Wiley & Sons.
65. Poudel, Y. R., Zhao, X., Jungjohann, K. L., Thapa, A., Guo, R., & Li, W. (2022). Ni3S2 nanowires filled carbon nanotubes of ultra-high quality: Synthesis methods, structure, and electrical properties. Diamond and Related Materials, 127, 109156.
66. Youn, H. C., Bak, S. M., Park, S. H., Yoon, S. B., Roh, K. C., & Kim, K. B. (2014). One-step preparation of reduced graphene oxide/carbon nanotube hybrid thin film by electrostatic spray deposition for supercapacitor applications. Metals and Materials International, 20, 975-981.
67. Smith, B. (2017). The CO bond, Part I: Introduction and the infrared spectroscopy of alcohols. Spectroscopy, 32(1), 14-21.
68. Mandal, S., Mandal, S., Ghosh, S. K., Sar, P., Ghosh, A., Saha, R., & Saha, B. (2016). A review on the advancement of ether synthesis from organic solvent to water. RSC advances, 6(73), 69605-69614.
69. Lin, W., Xiu, Y., Zhu, L., Moon, K. S., & Wong, C. P. (2008, May). Assembling of carbon nanotube structures by chemical anchoring for packaging applications. In 2008 58th Electronic Components and Technology Conference (pp. 421-426). IEEE.
70. Rahmam, S., Mohamed, N. M., & Sufian, S. (2014). Effect of acid treatment on the multiwalled carbon nanotubes. Materials Research Innovations, 18(sup6), S6-196.

71. De Menezes, B. R. C., Ferreira, F. V., Silva, B. C., Simonetti, E. A. N., Bastos, T. M., Cividanes, L. S., & Thim, G. P. (2018). Effects of octadecylamine functionalization of carbon nanotubes on dispersion, polarity, and mechanical properties of CNT/HDPE nanocomposites. Journal of materials science, 53(20), 14311-14327.
72. Kim, S. D., Kim, J. W., Im, J. S., Kim, Y. H., & Lee, Y. S. (2007). A comparative study on properties of multi-walled carbon nanotubes (MWCNTs) modified with acids and oxyfluorination. Journal of fluorine chemistry, 128(1), 60-64.
73. Wong, C. H., Buntov, E. A., Rychkov, V. N., Guseva, M. B., & Zatsepin, A. F. (2017). Simulation of chemical bond distributions and phase transformation in carbon chains. Carbon, 114, 106-110.
74. Ţucureanu, V., Matei, A., & Avram, A. M. (2016). FTIR spectroscopy for carbon family study. Critical reviews in analytical chemistry, 46(6), 502-520.
75. Zhang, C., Chang, J., Zhang, H., Li, C., & Zhao, H. (2019). Improved direct current electrical properties of crosslinked polyethylene modified with the polar group compound. Polymers, 11(10), 1624.
76. Teyssedre, G., & Laurent, C. (2005). Charge transport modeling in insulating polymers: from molecular to macroscopic scale. IEEE Transactions on Dielectrics and Electrical Insulation, 12(5), 857-875.
77. Wijeyasinghe, N., Eisner, F., Tsetseris, L., Lin, Y. H., Seitkhan, A., Li, J., ... & Anthopoulos, T. D. (2018). p-Doping of Copper (I) Thiocyanate (CuSCN) Hole-Transport Layers for High-Performance Transistors and Organic Solar Cells. Advanced Functional Materials, 28(31), 1802055.
78. Wijeyasinghe, N., & Anthopoulos, T. D. (2015). Copper (I) thiocyanate (CuSCN) as a hole-transport material for large-area opto/electronics. Semiconductor Science and Technology, 30(10), 104002.